HHS Public Access

Author manuscript

Nature. Author manuscript; available in PMC 2013 January 18.

Published in final edited form as:

Nature. 2010 October 28; 467(7319): 1074–1080. doi:10.1038/nature09487.

Homolog Structure of the SLAC1 Anion Channel for Closing Stomata in Leaves

Yuhang Chen[1,6], **Lei Hu**[2], **Marco Punta**[6,7], **Renato Bruni**[6], **Brandan Hillerich**[6], **Brian Kloss**[6], **Burkhard Rost**[1,6,1], **James Love**[6], **Steven A. Siegelbaum**[2,3,5], and **Wayne A. Hendrickson**[1,4,5,6]

[1]Department of Biochemistry and Molecular Biophysics, Columbia University, New York, NY 10032, USA

[2]Department of Neuroscience, Columbia University, New York, NY 10032, USA

[3]Department of Pharmacology, Columbia University, New York, NY 10032, USA

[4]Department of Physiology and Cellular Biophysics, Columbia University, New York, NY 10032, USA

[5]Howard Hughes Medical Institute, Columbia University, New York, NY 10032, USA

[6]NYCOMPS, New York Structural Biology Center 89 Convent Avenue, New York, NY 10027 USA

[7]Department of Computer Science and Institute for Advanced Study Technical University of Munich D-85748 Munich, Germany

Summary

The plant SLAC1 anion channel controls turgor pressure in the aperture-defining guard cells of plant stomata, thereby regulating exchange of water vapor and photosynthetic gases in response to environmental signals such as drought or high levels of carbon dioxide. We determined the crystal structure of a bacterial homolog of SLAC1 at 1.20Å resolution, and we have used structure-inspired mutagenesis to analyze the conductance properties of SLAC1 channels. SLAC1 is a symmetric trimer composed from quasi-symmetric subunits, each having ten transmembrane helices arranged from helical hairpin pairs to form a central five-helix transmembrane pore that is gated by an extremely conserved phenylalanine residue. Conformational features suggest a mechanism for control of gating by kinase activation, and electrostatic features of the pore coupled with electrophysiological characteristics suggest that selectivity among different anions is largely a function of the energetic cost of ion dehydration.

Correspondence and request for materials should be addressed to WAH (wayne@convex.hhmi.columbia.edu)..

Supplementary Information is linked to the online version of the paper at www.nature.com/nature.

Author Contributions YC, LH, MP, RB, BH, BK and JL performed experiments; YC, LH, BR, SAS, and WAH analyzed data; YC, LH, SAS, and WAH prepared the manuscript.

Author Information Atomic coordinates and diffraction data are deposited in the Protein Data Bank with accession codes 3M71, 3M73, 3M74, 3M75, 3M76, and 3M7L. See Table S4 for identifications. Reprints and permissions information is available at www.Nature.com/reprints.

Stomatal pores in the leaves of plants permit the influx of atmospheric carbon dioxide in exchange for transpirational evaporation of water[1,2]. A pair of kidney-shaped guard cells define each pore aperture, and turgor pressure variation in these cells determines the degree of stomatal pore openness. Depending on diverse environmental factors, the stomata close to prevent H_2O losses and open to admit CO_2 for photosynthesis. Environmental stimuli that lead to stomatal closure include darkness, high CO_2 levels, ozone, low air humidity and drought. The plant hormone abscisic acid (ABA) is critical for signal transduction from these stimuli. Mutational screens in *Arabidopsis thaliana* for CO_2 and ozone sensitivity identified a protein with ten predicted transmembrane (TM) helices, now called slow anion channel 1 (SLAC1), as having a central role in the control of stomatal closure[3-5]. Recent studies proved that SLAC1 is indeed an anion channel[6-7], with characteristics like those of slow anion channels found in guard cells[8], and that it is activated by phosphorylation from the OST1 kinase[9]. OST1 activity is negatively regulated by the ABI1 phosphatase[10,11], which is in turn inhibited by the stomatal ABA receptors PYR/RCAR[12,13] when in the ternary hormone-receptor-phosphatase complex[14-18]. Thereby, ABA stimulates SLAC1 channel activity. Resulting Cl^- efflux through SLAC1 causes membrane depolarization, which activates outward-rectifying K^+ channels, leading to KCl and water efflux to further reduce turgor and cause stomatal closure.

SLAC1 expression in *Arabidopsis* is confined to the guard cells of leaves, but other *Arabidopsis* tissues do have SLAC1 homologs[3], named SLAH1-SLAH4. The identifying mutations *slac1-1*[4] and *slac1-2*[3] are, respectively, in predicted transmembrane segments 9 (S456F) and 1 (G194D) of a protein that includes substantial N- and C-terminal extensions outside a 10-helix transmembrane (TM) domain. SLAH1, which is absent from leaves and lacks the terminal extensions of SLAC1, fully complements the mutant phenotype in *slac1-2* guard cell protoplasts[3]. SLAC1 and homologs are also present in other plant genomes, including nine in rice (*Oryza sativa*) and five in grape vines (*Vitis vinifera*). SLAC1 relatives, some quite remote, also occur in bacteria, archaea and fungi. Known prokaryotic homologs contain only the predicted transmembrane domain of SLAC1, but some fungal homologs do have N- and C-terminal extensions. One homolog, Mae1 from the yeast *Schizosaccharomyces pombe*, functions as a malate uptake transporter[19]; another, Ssu1 from *Saccharomyces cerevisiae* and other fungi including *Aspergillus fumigatus*, is characterized as a sulfite efflux pump[20,21]; and TehA from *Escherichia coli* is identified as a tellurite resistance protein by virtue of its association in the *tehA/tehB* operon[22,23]. Despite a lack of further biochemical characterization, many homologs are annotated as tellurite resistance/dicarboxylate transporter (TDT) proteins.

We have undertaken structural and functional characterizations of the SLAC1 anion channel. We first solved an atomic-resolution crystal structure of the TehA homolog from *Haemophilus influenzae*, and we then developed a homology model for *Arabidopsis* SLAC1. This model allowed us to conduct mutagenesis for functional testing of structure-inspired hypotheses on gating and selectivity. We expressed *Haemophilus* TehA and *Arabidopsis* SLAC1 in *Xenopus* oocytes to characterize channel properties of these proteins and mutant variants. We also determined crystal structures for several mutant variants, including the homolog of *slac1-2*.

Structure of SLAC1 bacterial homolog TehA

We performed a bioinformatic analysis of SLAC1-related proteins, first clustering nearly 900 non-redundant sequences into a superfamily at the PSI-BLAST level $E \leq 10^{-3}$, then into three distinct families at an initial threshold of $E \leq 10^{-30}$, and finally into subfamilies at a typical initial threshold of $E \leq 10^{-55}$. Since previous annotation is not well founded in experiment and SLAC1 is now the best characterized member, we adopt a nomenclature defining a SLAC superfamily divided into families identified as SF1-SF3 and subfamilies SF1A, SF1B etc. Family SF1 comprises the plant SLAC proteins and close bacterial homologs, family SF2 comprises a distinct set of bacterial proteins often annotated as exfoliative toxins, and family SF3 comprises the fungal Mae1 and Ssu1 proteins and their archaeal or bacterial homologs, respectively. SLAC family SF1 has three large subfamilies: the plant SLAC and SLAH proteins are in subfamily SF1A, closest bacterial homologs are in SF1B, and the TehA homologs are in SF1C (Fig. 1a). The other families also divide into subfamilies as detailed in Table S1, and family SF1 is divided into sub-subfamilies (Table S2). Two pertinent SF1 sequences are aligned in Fig. 1b.

We used a structural genomics approach to obtain structural information, testing expression and purification for 43 bacterial and archaeal likely homologs, assaying for detergent choice and stability on 8 of these, finding two with appropriate profiles by size exclusion chromatography, and obtaining suitable crystals for one. This protein, TehA from *H. influenzae* (*Hi*TehA), was found to be trimeric both by size-exclusion multi-angle light scattering (SEC-MALS) measurements and by chemical cross-linking. When solubilized in β-octylglucoside, *Hi*TehA crystallized in space group R3 with a=b=96.01Å and c=136.27Å. Each asymmetric unit contains one subunit and 65% solvent. The structure was solved by selenomethionyl (SeMet) SAD phasing, ultimately at 1.50Å resolution (Table S3, Fig. S1), and then refined at 1.20Å resolution (Fig. 2a) to R/R_{free} values of 14.1%/15.7% for a model that includes ordered residues 6-313, 213 water molecules and four detergent molecules (Table S4).

The crystal structure has TehA trimers aligned with three-fold axes of the lattice (Fig. 2b). Subunits are tightly associated, burying 8947 $Å^2$ of total surface area within trimer interfaces. The electrostatic potential surface is largely negative on the extracellular surface (Fig. 2c) and largely positive on the cytoplasmic surface (Fig. 2d). The membrane orientation is specified experimentally from GFP tagging of *E. coli* TehA[24]. Each TehA protomer has ten TM helices, as predicted; however, the fold is novel. Tandemly repeated helical hairpins are arranged with quasi-five-fold symmetry (Figs. 2e,S2). Extracellular inter-helix loops are short (2-5 residues) whereas intracellular inter-helix connections are longer, including a nine-residue helix $H_{2,3}$ between TM_2 and TM_3 (Fig. 2f). An inner pentad of outwardly directed, TM_{odd}, helices creates an apparent pore through each protomer perpendicular to the putative membrane plane. TM_{even} helices from the five hairpins surround the inner pore and make an outer layer.

Homology model for plant SLAC1

Arabidopsis SLAC1 (*At*SLAC1) is substantially similar to bacterial homologs, notably *Hi*TehA (Fig. 1b). All *Hi*TehA TM helices are fully aligned to predicted SLAC1 TM helices, but there are short inter-helical gaps (1-5 residues) in all five extracellular loops and in two of the intracellular loops. The TM domain of *At*SLAC1 (residues 188-504) aligns to *Hi*TehA with 19% sequence identity and with a PSI-BLAST E-value of 3×10^{-22}. For comparison, and in keeping with the family tree (Fig. 1a), the TM domain of *At*SLAC1 shares sequence identities of 76% with rice SLAC1, 41% with *Arabidopsis* SLAH1, 25% with an SL1B homolog from *Halorhodospira halophila*, 11% with *S. cerevisiae* Ssu1, and 9% with *S. pombe* Mae1. A conceptual model with the *At*SLAC1 sequence transposed onto the *Hi*TehA helices sufficed to guide most of our mutational tests, but a detailed *At*SLAC1 homology model helped to refine our ideas. Surface variability and electrostatic potential are plotted onto the surface of this model (Fig. 2g,2h).

The most remarkable feature of the TehA structure and corresponding SLAC1 model is the central pore through each protomer. As for acetylcholine receptors[25], the SLAC1 pore is formed by five helices; but the SLAC1 helices come from one protein molecule rather than five. The SLAC1 pore has a relatively uniform diameter of approximately 5Å across nearly five helical turns (Fig. S3), except for a pronounced constriction in the middle of the membrane (Fig. 3a) where the pore is occluded by the side chain of Phe 450 (Phe 262 in *Hi*TehA). This residue is the only absolutely conserved amino acid residue of the SLAC1 family. The pore is lined with highly conserved (86% identity among five SLAC1 orthologs; 32% identity between *At*SLAC1 and *Hi*TehA) and generally hydrophobic residues (Figs. 1b, 3b,3c,S4). Despite this hydrophobicity, the electrostatic potential on the pore surface is polarized (Fig. 3a), presumably due to an invaginated shape adjacent to charged residues outside the membrane. The generally electropositive character of the cytoplasmic surface likely contributes to anion efflux.

Kinks in the pore helices contribute to formation of a relatively constant pore diameter across the membrane. Four of the five *Hi*TehA inner helices have centrally located proline residues, which necessarily generate kinks, and TM_9 is kinked at a backbone-coordinated water molecule (Fig. 3d). Proline replaces Gly263 in all SF1A and SF1B relatives, including Pro451 *At*SLAC1. This water-displacing change is isostructural[26]. Centrally located prolines also prevail in TM_3, TM_5 and TM_7 across the SF1 proteins. The outer helices are longer and straighter, but more inclined. The only outer-helix proline kink of *Hi*TehA is in TM_6 at the trimer three-fold axis.

Two of the gene-identifying mutations in *Arabadopsis* SLAC1 are selected point mutations, others are disruptive transfer DNA (T-DNA) insertions[4]. In the *At*SLAC1 homology model, the *slac1-2* (G194D) mutation[3] points into the pore from TM_1 and can be accommodated structurally whereas the *slac1-1* (S456F) mutation[4] points away from the pore six residues after pore-blocking Phe450 on TM_9 and would be expected to disruptive. Ser456 interacts with outer helix TM_{10} in the homology model, and the phenyl bulk from S456F would not fit. Position 456 has alanine in *Hi*TehA, 66% of all 204 SF1 homologs and another 27% have threonine or serine (as in all SLAC1 channels); phenylalanine never occurs among all

814 SLAC superfamily members. Position 194 has glycine in 58% of SF1 homologs and alanine in another 22%. Asp194, which never occurs naturally, would block the pore and be expected to repel anions.

Mutational tests of channel function

Mutational studies corroborate the hypothesis that a TehA-based SLAC1 model is appropriate. First, as discussed above, the *slac1-1* mutant (S456F) is expected to be structurally disruptive, and indeed it is inactive in guard cells[4], and the *slac1-2* mutation (G194D) is expected to block the pore, and we show below that this variant is also inactive. We have also shown that the introduction of SLAC1-conserved proline residues into *Hi*TehA (A208P/G263P) is accommodated isomorphously[26]. Moreover, as shown below, channel conductance properties of several mutants are similar for *At*SLAC1 and *Hi*TehA.

To examine characteristics of the SLAC1 channel in light of the structural model, we performed electrophysiological tests of membrane currents from voltage-clamped *Xenopus* oocytes following injection of wild-type or mutant *At*SLAC1 or *Hi*TehA cRNAs. We observed modest-sized chloride currents with wild-type *At*SLAC1 cRNA, as found previously[6,7], but did not detect any chloride current following injection of wild-type *Hi*TehA cRNA. We found that SLAC1 Cl^- conductance was enhanced when the OST1 kinase cRNA was co-injected with SLAC1 cRNA, but only to the levels found by Lee et al.[6] and not to the much higher levels found by Geiger et al.[7] with OST1 physically connected to SLAC1 by split YFP linkage. In keeping with structural evidence that Phe262 blocks the *Hi*TehA pore, removal of the phenyl group in *Hi*TehA F262A or in the homologous *At*SLAC1 F450A resulted in very large Cl^- currents relative to wild-type levels, and the SLAC1 currents were now less enhanced by presence of OST1 (Fig. 4a). The tempting interpretation of an opened gate will require validation with appropriately analyzed single-channel recordings[27]. In keeping with the *slac1-2* phenotype[3], neither the functionally impaired *At*SLAC1 G194D nor its *Hi*TehA G15D homolog showed any substantial conductance; moreover, further consistent with pore blockage by Asp194 in *slac1-2*, the large conductances of *Hi*TehA F262A and *At*SLAC1 F450A were stopped in the double mutants *At*SLAC1 G194D/F450A and *Hi*TehA G15D/F262A (Fig. 4a). Here again, the effects in SLAC1 were independent of OST1.

We also tested conductance characteristics for a series of *At*SLAC1 F450X substitution mutants – F450A,G,T,V,L– and for the corresponding *Hi*TehA F262X series – F262A,G,T,V,L (Figs. 4b,S5, Table S5). Findings from the two series are roughly parallel; in particular, the alanine and glycine substitutions lead to large currents for both and in comparison to the others. There are distinctions, of course, including generally higher conductances for *At*SLAC1 over *Hi*TehA and less conductance of F262T TehA compared to F450T SLAC1. It is also noteworthy that OST1 activation is very muted for the F450A,G,L mutants, which is consistent with SLAC1 gating at Phe450.

Crystal structures were also determined for several of the *Hi*TehA mutant variants (Table S4). The structures of F262A (1.15Å), F262V (1.60Å), F262L (1.65Å) and G15D (1.50Å) are all essentially isomorphous with the wild-type TehA structure with changes localized

primarily at the sites of mutation; the same is true for the double mutations of F262A/G15D, F262G/G15D and A208P/G263P[26]. The F262A structure has a wide open pore (Fig. 5a) with a relatively uniform pore diameter of ~5Å through ~30Å across the membrane (Fig. S3) whereas G15D has a doubly occluded pore (Fig. 5b). The pores of other mutant variants are consistent with the sizes of constrictive residues and with the observed conductances.

Gating and activation

The crystal structures of TehA and its mutant variants when taken together with the functional studies in *Xenopus* oocytes point to a crucial role for Phe450 in gating of the SLAC1 anion channel. Conservation of this residue across the SLAC1 family implies functional importance. The occlusion of the pore by the presence of F262 in the structure of wild-type TehA and the openness of the pore upon its substitution by alanine in the structure of the F262A mutant provides physical evidence for a gating role of this residue. This interpretation is supported by the correlated conductance characteristics from variants of the *At*SLAC1 and *Hi*TehA channels (Figs. 4b,S5). While these observations may suffice for placing the gate within the channel pore, they do not by themselves suggest a mechanism for gating in response to physiological stimuli. Some insight does come from conformational details defined at high resolution.

One important structural clue is that the side chain of Phe262 is in a high energy conformation in the *Hi*TehA structure, with χ_1/χ_2 at −160°/-4°. Although χ_1 is in a preferred *trans* conformation, the phenyl ring is restricted by contacts with Val210 and Leu18 to a χ_2 value near 0° rather than near to the preferred 90° orientation (Fig. 5c). Further evidence that Phe262 is restrained from local equilibrium comes from shifts observed in crystal structures of the F262A, F262V, F262L and F262G/G15D variants, which all show consistent backbone movements that displace Cβ(262) by 0.47-0.78Å (Fig. 5d). By contrast, Leu262 in F262L is in a preferred trans/gauche$^+$ conformation at χ_1/χ_2 = 177°/63° as is Val262 in F262V at χ_1 = −176°. What might control activation of *Hi*TehA is unclear, but for *At*SLAC1 activation is by OST1 phosphorylation[6,7]. The molecular consequences of OST1 phosphorylation of SLAC1 remain unknown, but it is plausible that associated shifts in pore-helix orientations would unlatch Phe450 in SLAC1 from a TehA-like restrained orientation. By analogy with Leu262 in F262L, we expect a preferred rotameric state for Leu450 in *At*SLAC1 F450L. Thus, the lack of appreciable OST1 activation of conductance in *At*SLAC1 F450L (Fig. 5e) might be explained by the lack of a restraining latch, whereby the channel remains closed despite OST1 activation. Puzzles certainly remain since OST1 does substantially activate *At*SLAC1 F450T or F450V, which like *Hi*TehA F262V should also be unrestrained; presumably activating adjustments widen the pore enough for ion permeation past threonine and valine but not leucine.

Phosphorylation sites have been discovered in the N- and C-terminal tails of *At*SLAC1[6,7,28] (179 and 51 residues long, respectively), but these alone cannot explain OST1 activation of SLAC1. First SLAH1, which fully complements the *slac1-1* mutation, does not have these cytoplasmic tails. Secondly, although OST1 phosphorylation of Ser120 in the N-terminal tail is necessary for SLAC1 activation, it is not sufficient[7]. Thus, we surmise that direct phosphorylation of the SLAC1 TM domain must be critical, and SLAC1 has four conserved

Ser/Thr candidates in its cytoplasmic loops. Moreover, SLAC1 proteins have proline-mediated kinks at the putative Phe450 gate in helix TM_9, and also in adjacent helix TM_7; these features may play a role in phosphorylation-driven unlatching of the Phe450 gate in SLAC1.

Ion selectivity and discrimination

Our studies of SLAC1 channel relative ion permeabilities, based on measurements of current reversal potential, are consistent with earlier work demonstrating that *At*SLAC1 conducts anions but not cations and is selective among anions, with greater permeability for nitrate than for chloride (as in *Vicia faba* guard cell protoplasts[27]) and much reduced permeability for malate, bicarbonate or sulfate[6,7]. We also find that SLAC1 has little permeability for sulfite. Additionally, we find that wild-type SLAC1, F450A and F450T all have similar relative permeabilities to chloride, sulfite and malate, despite having widely different conductance levels, but the gating mutants do show small but significant decreases in nitrate permeability (Fig. 4c, Table S6).

The relative insensitivity of anion permeability to gating residue changes suggests that selectivity for these anions may occur away from the central constriction at the channel gate. To some extent, ionic discrimination must depend on pore geometry; thus, an organic anion such as malate may be simply too large to pass through the 5-Å wide pore. Although the SLAC1 pore is lined largely with hydrophobic sidechains (Fig. 3c), it is sprinkled with hydroxyl groups from serine and threonine residues (16%); their electropositive hydrogen atoms may facilitate conductance. Most strikingly, the electrostatic potential within the *At*SLAC1 pore is electropositive throughout (Fig. 3a). This polarization, promoted by charges on extra-membranous loops, no doubt contributes significantly in discrimination against cations.

The relative anion permeability sequence of SLAC1 determined by us and others, $I^- > NO_3^- > Br^- > Cl^-$ [6,7], corresponds to selectivity sequence 1 compiled by Wright and Diamond[29] for a range of anion-selective proteins. This sequence correlates inversely with the hydration energies of monovalent anions – anions with a lower hydration energy have a greater channel permeability. It is thought to be generated in proteins with weak, low field-strength, anion binding sites, where selectivity is largely determined by the energetic cost of anion dehydration. These selectivity results are thus consistent with the SLAC1 structure, where the pore lacks any obvious anion binding site.

Distinctiveness of the SLAC1 channel

SLAC1 anion channels are entirely novel in structure and, apparently, in the mechanism for ion conductance. The best characterized of anion channels belong to the CLC family of Cl^- channels and transporters[30-32]. CLC channels have an altogether different architecture from the SLAC1 channel, and the mechanism for selectivity is also very different. Bacterial CLC transporters bind halide ions at three sites in a highly constricted pore[30]. By contrast, the SLAC1 pore has a relatively uniform diameter across the membrane, except where closed by the gating phenyl group, and we do not find discrete ion binding sites. CLC selectivity is governed by specific residues surrounding these binding sites[30,32]. The anion selectivity

sequence for the CLC channels of $Cl^{-}>Br^{-}>NO^{-}_{3}>I^{-}$, opposite of that in SLAC1, is consistent with the high field-strength anion binding sites in CLC channels[29]. Interestingly, as for *At*SLAC1, an *Arabidopsis* CLCa channel also preferentially transports nitrate ions[33], and an *E. coli* CLC channel is converted to preference of nitrate when a generally conserved serine at the central site is substituted with proline as in *At*CLCa[32].

SLAC1 also differs radically from other structurally characterized anion channels and transporters. These include the VDAC1 voltage-gated anion channel from mitochondrial outer membranes, which has a porin-like beta-barrel structure[34-36], and a light-driven halorhodopsin chloride pump, which has a transmembrane conductance pathway similar to that of the proton-pumping pore of bacteriorhodopsin[37]. Although its channel structure is still only known by homology to other ABC transporters, CFTR is another obviously distinct chloride channel[38]. Cys-loop receptors also include anion channels[39], and these are similar to SLAC1 in having five-helix pores[25], but here selectivity is governed by charged groups at the entrance to the pore, which distinguish the anion-selective $GABA_A$ and glycine receptors from the cation-selective acetylcholine and serotonin 5HT3 receptors[39]. Finally, the recently identified TMEM16A gene for calcium-activated chloride channels[40-42] appears to encode an 8-TM protein that is again distinct from SLAC1.

Stomatal guard cells show both rapidly activated (R-type) and slow (S-type) anion channel activity[43]. Although *slac1* guard cells have very defective S-type activity, their R-type currents are normal[4]. Guard cell protoplasts from the *slac1-2* mutant abnormally accumulate Cl^{-}, K^{+}, malate and fumarate[3], whereas SLAC1 shows negligible malate conductance[7]. As for SLAC1-associated K^{+} movements, other channels or transporters must be responsible for SLAC1-associated malate movements. Recent studies indicate that *At*ALMT12, an aluminium-activated malate transporter (ALMT) family member, is a malate-dependent R-type anion channel[44] needed for stomatal closure[45].

Conclusions

We find that many functional properties of the plant SLAC1 anion channel are explained well by the structure of an uncharacterized bacterial TehA protein that has been associated with tellurite resistance. SLAC1 and TehA belong to distinct subfamilies within one branch of a larger SLAC1 superfamily, but *At*SLAC1 and *Hi*TehA are sufficiently similar (19% sequence identity) that the SLAC1 homology model is predictive for function, including a verified placement of the identifying *slac1-2* mutation G194D and a phenylalanine gate. One remaining puzzle concerns the structural change that activating phosphorylation elicits in SLAC1, and another puzzle is the biochemical role of the TehA homologs in bacteria. In a companion paper[26], we examine functional and structural properties of TehA in bacteria, showing that it is anion channel, although actually not conferring tellurite resistance, and identifying a mutant variant with properties suggestive of an activated state. Thus, SLAC1 and TehA likely represent a large family of selective anion channels controlled by environmental stimuli.

METHODS

Selection of target sequences

TehA from *E. coli* (*Ec*TehA) was a centrally selected sequence for expansion as a NYCOMPS targeted family. Target selection criteria utilized at NYCOMPS are described in details elsewhere[46]. Briefly, the *Ec*TehA sequence was run against a dataset of about 40,000 predicted alpha helical integral membrane protein sequences from prokaryotic genomes (NYCOMPS98 dataset[46]) using PSI-BLAST[50]. Sequences that matched *Ec*TehA with an E-value lower than 10^{-3} in an alignment extending over at least 50% of both predicted TM regions and passing our post-seed-expansion filtering criteria[46] were passed to the protein production pipeline.

Protein expression screening

Full-length homologs from the following 38 species, including 2 sequences each from 5 of these, were amplified from genomic DNA by PCR: *Thermoplasma acidophilum*, *Lactococcus lactis* subsp. lactis Il1403, *Streptococcus pyogenes* M1 GAS, *Streptococcus pneumoniae* TIGR4, *Haemophilus influenzae* Rd KW20, *Methanocaldococcus jannaschii* DSM 2661 (2), *Escherichia coli* K12, *Salmonella typhimurium* LT2, *Clostridium perfringens* ATCC 13124, *Xanthomonas campestris* pv. campestris str. ATCC 33913, *Streptococcus agalactiae* 2603V/R, *Shewanella oneidensis* MR-1, *Streptococcus mutans* UA159, *Archaeoglobus fulgidus* DSM 4304, *Vibrio parahaemolyticus* RIMD 2210633 (2), *Pseudomonas syringae* pv. tomato str. DC3000 (2), *Enterococcus faecalis* V583, *Pyrococcus horikoshii* OT3, *Bordetella bronchiseptica* RB50, *Streptomyces coelicolor* A3, *Corynebacterium glutamicum* ATCC 13032, *Picrophilus torridus* DSM 9790, *Acinetobacter* sp. ADP1, *Vibrio fischeri* ES114, *Pseudomonas fluorescens* Pf-5, *Sulfolobus acidocaldarius* DSM 639, *Colwellia psychrerythraea* 34H, *Neisseria meningitidis* MC58, *Rhodobacter sphaeroides* 2.4.1, *Vibrio cholerae* O1 biovar eltor str. N16961 (2), *Marinobacter aquaeolei* VT8, *Acinetobacter baumannii* ATCC 17978, *Klebsiella pneumoniae* subsp. pneumoniae MGH 78578, *Streptomyces avermitili* MA-4680, *Bordetella parapertussis* 12822 (2), *Streptococcus thermophilus* LMG 18311, *Salmonella enterica* subsp. enterica serovar Paratyphi A str. ATCC 9150, and *Anaeromyxobacter dehalogenans* 2CP-C.

Selected cDNAs were cloned into a modified pET vector (Novagen, Inc) that fuses a FLAG and deca-histidine tag at the C-terminus, which are cleavable by TEV protease. Proteins were expressed in *E. coli* BL21(DE3) plysS by a high throughput format (0.6ml in a deep well block) and purified after lysis by sonication using metal affinity purification in a buffer containing N-Dodecyl-β-D-Maltopyranoside. Samples were passed over an analytical size exclusion column in 12 different detergent-containing mobile phases, which included N-dodecyl-β-D-maltopyranoside (DDM), N-decyl-β-D-altopyranoside (DM), N-nonyl-β-D-altopyranoside (NM), N-octyl-β-D-altopyranoside (OM), N-octyl-β-D-Glucopyranoside (OG), N-nonyl-β-D-Glucopyranoside (NG) and lauryl dimethyl amine oxide (LDAO). Multi-angle light scattering with refractive index detection was used to analyze the oligomeric state[51]. The *E. coli* and *H. influenzae* proteins were judged to be monodisperse and stable and were passed to scale up.

Scaled-up production and purification

For scale up, in brief, transformed BL21 plysS cells were grown at 37°C in 2× YT media to OD 0.6-0.8 after being inoculated with 1% of the overnight culture. The culture was induced with 0.4mM IPTG and continued to grow at 37 °C for another 4 hours. The cells were harvested by centrifugation and stored at −80°C before use. Selenomethionyl (SeMet) TehA was expressed in a similar way, but using containing SeMet in place of methionine in defined minimal media. Cells were resuspended in a buffer containing 50 mM Tris-HCl (pH 8.0) and 200 mM NaCl and lysed using a French Press with two passes at 15-20,000 psi. Cell debris were removed by centrifugation at 10,000g for 20min, and the membrane fraction was isolated from that supernatant by ultra-centrifugation at 150,000g for 1 hr.

The membrane fraction was homogenized in a solubilization buffer containing 50 mM Tris (pH 8.0) and 200 mM NaCl, and incubated with final concentration of 1% (w/v) dodecyl-β-D-maltopyranoside (DDM, Anatrace, Inc) for 1 hr at 4°C. The non-dissolved matter was remove by ultracentrifugation at 150,000g for 30 min, and the supernatant was loaded to a 5ml Hitrap Ni^{2+}-NTA affinity column (GE Healthcare), pre-equilibrated with the same solubilization buffer supplemented with 0.05% DDM. After 20 column volume buffer wash, the protein was eluted with 250mM imidazole in the solublization buffer. The Flag and 10-His tags were removed by adding super TEV at 1:100 mass ratio and incubating at 4°C overnight. Tag removal was confirmed by SDS-PAGE, and the resulting sample was concentrated to around 10mg/ml. Preparative size exclusion chromatography was carried out on a Superdex-200 column for further purification, removal of TEV protease and the cleaved tag, and for buffer and detergent exchange. The gel-filtration buffer contained 10 mM Tris (pH 8.0), 200 mM NaCl, 1mM EDTA, 0.5 mM Tris [2-carboxyethyl] phosphine **(**TCEP), and 2×CMC of detergent. In the case of *Hi*TehA, the protein was well behaved and stable in nearly all tested detergents, and we have purified it from DDM, DM, NM, OM, OG and LDAO.

Protein characterization

We performed N-terminal amino-acid sequencing of purified HiTehA and EcTehA prior to TEV protease treatment. Results from these analyses proved that true initiating methionine residue is located 14 residues after one annotated as N-terminal. The intervening nucleotide sequence contains a Shine-Delgarno sequence.

For cross-linking experiments, purified *Hi*TehA was incubated with 10 mM disuccinimidyl glutarate at room temperate for 30 min, and 100mM Tris-HCl pH 7.5 was added to stop the reaction. The incubated sample when run on a 8-25% gradient SDS-PAGE gel showed a ladder consistent with a trimeric structure.

Crystallization and data collection

Purified protein was concentrated to ~10mg/ml for initial crystal trials in a Mosquito robot with commercial screens from Hampton research, Emerald Biosystems and Molecular Dimension. We obtained crystals of *Hi*TehA from protein in detergent DDM, DM, NM, OM, OG and LDAO, but only those from LDAO and OG gave diffraction to beyond 4Å spacings. Crystals that proved useful were all grown at 4°C using the sitting-drop vapor

diffusion method. After extensive optimization we reached conditions supporting very high resolution. Wild-type *Hi*TehA and most of its variants crystallized from 1mM $ZnSO_4$, 50mM Hepes-Na pH 7.8 and 28% PEG600. *Hi*TehA F262A crystallized from 200mM Li_2SO_4, 100mM glycine pH9.3 and 33% PEG400). Addition of 10mM spermidine as an additive helped to obtain slightly better diffracting crystals. Cryoprotection was achieved by adding 5% ethylene glycol or PEG400 to the crystallization solution.

Structure determination and refinement

Native and SeMet SAD data set were collected at NSLS beamline X4A and processed using the software HKL2000[52]. Crystals of *Hi*TehA grew in space group R3 with a=b=c = 85.0Å and α=β=γ = 93.5°. All subsequent manipulations were done in the hexagonal setting of this space group with a=b= 96.0Å and c = 136.7Å. The asymmetric unit contains one TehA protomer and 65% solvent volume. The structure was determined at 2.0Å resolution from single-wavelength anomalous diffraction (SAD) using selenomethionine-substituted protein crystals. Assessment of data quality for phasing, location of heavy atom sites and initial phases were calculated using the HKL2MAP interface to SHELX programs[53].

All the secondary structure elements were clearly visible in the experimental electron density map. Automatic model building was done in Arp/wArp[54] and completed manually in the program COOT[55]. The model was refined against native data at 1.20Å resolution using the program Refmac5.5 in CCP4[56], with anisotropic B factor restrained refinement applied. Subsequent structural analyses of mutant variants were refined as isomorphous structures.

Site-directed mutagenesis

Site-directed mutants were constructed using the QuikChange Site-Directed Mutagenesis Kit (Stratagene, La Jolla, CA 92037) and expressed from pET vectors in *E. coli* BL21(DE3) plysS cells as for the wild-type protein.

Electrophysiology

All constructs were cloned into plasmid pGHME2, linearized, and transcribed into cRNA using T7 polymerase (mMessage mMachine, Ambion). Oocytes were injected with 50 nl of cRNA solution each, at a constant concentration of 0.5 mg/ml for *Hi*TehA, or 0.5 mg/ml for *At*SLAC1 constructs, with or without 0.5 mg/ml of *At*OST1 constructs and recorded in voltage-clamp experiments 2 days after injection. For mixed expression experiments, 25nl of cRNA solution was injected for each *At*SLAC1 component. Two-electrode voltage clamp recordings were performed to measure *Hi*TehA or *At*SLAC1 currents as described[6,7]. The pipette solutions contained 3 M KCl. For voltage-clamp current recordings, the bath solution contained 1 mM $MgCl_2$, 1 mM $CaCl_2$, 10 mM Mes/Tris (pH 5.6) and 30 mM CsCl; For anion selectivity measurements, the bath solutions contained 50 mM Cl^-, NO^-_3, malate, or 30 mM SO^{2-}_3 sodium salts, 45 mM Na-gluconate, 1 mM Ca-$gluconate_2$, 1 mM Mg-$gluconate_2$, 1 mM K-gluconate, as well as 10 mM Tris/Mes (pH 5.6). Osmolality was adjusted with D-mannitol to 220 mOsmol/kg. The bath electrode was a 3M KCl agar bridge. The testing potentials were +50 to −110 or −130 mV in 20 mV decrements with 7.5 s duration. The holding and return potentials were 0 mV with a 1.45 s or 2 s, respectively. I-V

relations of *Hi*TehA or *At*SLAC1 were generated from the current reached after 0.5 s in testing potentials. The Goldman-Hodgkin-Katz equation was applied to estimate permeability ratios for monovalent ions as described[6]. For divalent anions, the permeability ratios were derived according to Fatt and Ginsborg[57].

Bioinformatic analysis of SLAC-related proteins

Sequences related to SLAC1 were analyzed comprehensively by PSI-BLAST[50]. Searches at $E<10^{-3}$ starting from five disparate homologs each identified a common pool of over 900 proteins, which when pooled were used for sub-classification into families and subfamilies. Details of these analyses are reported in footnotes to Table S1.

Molecular figures were produced in PyMOL[58].

Supplementary Material

Refer to Web version on PubMed Central for supplementary material.

Acknowledgments

We thank Filippo Mancia, Larry Shapiro and Ming Zhou for helpful discussions; Patricia Rodriguez and Arianne Morrison for help with cloning and expression; Jonah Cheung, Mark Collins, Chris Min, Sheng Ye and Zhen Zhang for advice in protein chemistry and crystallography; John Schwanof and Randy Abramowitz for help with synchrotron experiments; John Riley for help with *Xenopus* oocyte injections; and Min Su for advice on the PSI-BLAST analysis of SLAC relatives. This project was supported in part by an award to the New York Consortium on Membrane Protein Structure (NYCOMPS) from the NIGMS Protein Structure Initiative. Beamline X4A at the National Synchrotron Light Source (NSLS), a DOE facility at Brookhaven National Laboratory, is supported by the New York Structural Biology Center.

References

1. Hetherington AM, Woodward FI. The role of stomata in sensing and driving environmental change. Nature. 2003; 424:901–908. [PubMed: 12931178]
2. Sirichandra C, Wasilewska A, Vlad F, Valon C, Leung J. The guard cell as a single-cell model towards understanding drought tolerance and abscisic acid action. J. Exp. Bot. 2009; 60:1439–1463. [PubMed: 19181866]
3. Negi J, et al. CO_2 regulator SLAC1 and its homologues are essential for anion homeostatsis in plant cells. Nature. 2008; 452:483–486. [PubMed: 18305482]
4. Vahisalu T, et al. SLAC1 is required for plant guard cell S-type anion channel function in stomatal signalling. Nature. 2008; 452:487–491. [PubMed: 18305484]
5. Saji S, et al. Disruption of a gene encoding C4-dicarboxylate transporter-like protein increases ozone sensitivity through deregulation of the stomatal response in Arabidopsis thaliana. Plant Cell Physiol. 2008; 49:2–10. [PubMed: 18084014]
6. Lee SC, Lan W, Buchanan BB, Luan S. A protein kinase-phophatase pair interacts with an ion channel to regulate ABA signaling in plant guard cells. Proc. Natl. Acad. Sci. USA. 2009; 106:21419–21424. [PubMed: 19955427]
7. Geiger D, et al. Activity of guard cell anion channel SLAC1 is controlled by drought-stress signaling kinase-phosphatase pair. Proc. Natl. Acad. Sci. USA. 2009; 106:21425–21430. [PubMed: 19955405]
8. Schroeder JI, Hagiwara S. Cytosolic calcium regulates ion channels in the plasma membrane of Vicia faba guard cells. Nature. 1989; 338:427–430.
9. Mustilli A, Merlot S, Vavasseur A, Fenzi F, Giraudat J. Arabidopsis OST1 protein kinase mediates the regulation of stomatal aperture by abscisic acid and acts upstream of reactive oxygen species production. Plant Cell. 2002; 14:3089–3099. [PubMed: 12468729]

10. Leung J, et al. Arabidopsis ABA response gene ABI1: features of a calcium-modulated protein phosphatase. Science. 1994; 264:1448–1452. [PubMed: 7910981]
11. Meyer K, Leube MP, Grill E. A protein phosphatase 2C involved in ABA signal transduction in Arabidopsis thaliana. Science. 1994; 264:1452–1455. [PubMed: 8197457]
12. Ma Y, et al. Regulators of PP2C phosphatase activity function as abscisic acid sensors. Science. 2009; 324:1064–1068. [PubMed: 19407143]
13. Park S, et al. Abscisic acid inhibits type 2C protein phosphatases via the PYR/PYL family of START proteins. Science. 2009; 324:1068–1071. [PubMed: 19407142]
14. Melcher K, et al. A gate-latch-lock mechanism for hormone signalling by abscisic acid receptors. Nature. 2009; 462:602–608. [PubMed: 19898420]
15. Miyazono K, et al. Structural basis of abscisic acid signalling. Nature. 2009; 462:609–614. [PubMed: 19855379]
16. Fujii H, et al. In vitro reconstitution of an abscisic acid signalling pathway. Nature. 2009; 462:660–664. [PubMed: 19924127]
17. Yin P, et al. Structural insights into the mechanism of abscisic acid signaling by PYL proteins. Nat. Struct. Mol. Biol. 2009; 16:1230–1236. [PubMed: 19893533]
18. Nishimura N, et al. PYR/PYL/RCAR family members are major in-vivo ABI1 protein phosphatase 2C-interacting proteins in Arabidopsis. Plant J. 2010; 61:290–299. [PubMed: 19874541]
19. Grobler J, Bauer F, Subden RE, van Vuuren HJ. The MAE1 gene of Schizosaccharomyces pombe encodes a permease for malate and other C4 dicarboxylic acids. Yeast. 1995; 11:1485–1491. [PubMed: 8750236]
20. Park H, Bakalinsky AT. SSU1 mediates sulphite efflux in Saccharomyces cerevisiae. Yeast. 2000; 16:881–888. [PubMed: 10870099]
21. Léchenne B, et al. Sulphite efflux pumps in Aspergillus fumigatus and dermatophytes. Microbiology. 2007; 153:905–913. [PubMed: 17322211]
22. Walter EG, Weiner JH, Taylor DE. Nucleotide sequence and overexpression of the tellurite-resistance determinant from the IncHII plasmid pHH1508a. Gene. 1991; 101:1–7. [PubMed: 2060788]
23. Taylor DE, Hou Y, Turner RJ, Weiner JH. Location of a potassium tellurite resistance operon (tehA tehB) within the terminus of Escherichia coli K-12. J Bacteriol. 1994; 176:2740–2742. [PubMed: 8169225]
24. Daley DO, et al. Global topology analysis of the Escherichia coli inner membrane proteome. Science. 2005; 308:1321–1323. [PubMed: 15919996]
25. Unwin N. Refined structure of the nicotinic acetylcholine receptor at 4Å resolution. J. Mol. Biol. 2005; 346:967–989. [PubMed: 15701510]
26. Chen Y, Hu L, Siegelbaum SA, Hendrickson WA. Structure-based analysis of anion channel TehA and methyltransferase TehB implicated in bacterial tellurite resistance. Submitted.
27. Schmidt C, Schroeder JI. Anion Selectivity of Slow Anion Channels in the Plasma Membrane of Guard Cells (Large Nitrate Permeability). Plant Physiol. 1994; 106:383–391. [PubMed: 12232336]
28. Vahisalu T, et al. Ozone-triggered rapid stomatal response involves the production of reactive oxygen species, and is controlled by SLAC1 and OST1. Plant J. 2010; 62:442–53. [PubMed: 20128877]
29. Wright EM, Diamond JM. Anion selectivity in biological systems. Physiol. Rev. 1977; 57:109–156. [PubMed: 834775]
30. Dutzler R, Campbell EB, MacKinnon R. Gating the selectivity filter in ClC chloride channels. Science. 2003; 300:108–112. [PubMed: 12649487]
31. Accardi A, Miller C. Secondary active transport mediated by a prokaryotic homologue of ClC Cl-channels. Nature. 2004; 427:803–807. [PubMed: 14985752]
32. Picollo A, Malvezzi M, Houtman JC, Accardi A. Basis of substrate binding and conservation of selectivity in the CLC family of channels and transporters. Nat. Struct. Mol. Biol. 2009; 16:294–301. [PubMed: 19219045]
33. De Angeli A, et al. The nitrate/proton antiporter AtCLCa mediates nitrate accumulation in plant vacuoles. Nature. 2006; 442:939–942. [PubMed: 16878138]

34. Hiller S, Garces RG, Malia TJ, Orekhov VY, Colombini M, Wagner G. Solution structure of the integral human membrane protein VDAC-1 in detergent micelles. Science. 2008; 321:1206–1210. [PubMed: 18755977]
35. Bayrhuber M, et al. Structure of the human voltage-dependent anion channel. Proc. Natl. Acad. Sci. USA. 2008; 105:15370–15375. [PubMed: 18832158]
36. Ujwal R, et al. The crystal structure of mouse VDAC1 at 2.3 Å resolution reveals mechanistic insights into metabolite gating. Proc. Natl. Acad. Sci. USA. 2008; 105:17742–17747. [PubMed: 18988731]
37. Kouyama T, et al. Crystal structure of the light-driven chloride pump halorhodopsin from Natronomonas pharaonis. J. Mol. Biol. 2010; 396:564–579. [PubMed: 19961859]
38. Gadsby DC, Vergani P, Csanády L. The ABC protein turned chloride channel whose failure causes cystic fibrosis. Nature. 2006; 440:477–483. [PubMed: 16554808]
39. Miller PS, Smart TG. Binding, activation and modulation of Cys-loop receptors. Trends Pharmacol. Sci. 2010; 31:161–174. [PubMed: 20096941]
40. Yang YD, et al. TMEM16A confers receptor-activated calcium-dependent chloride conductance. Nature. 2008; 455:1210–5. [PubMed: 18724360]
41. Caputo A, et al. TMEM16A, a membrane protein associated with calcium-dependent chloride channel activity. Science. 2008; 322:590–594. [PubMed: 18772398]
42. Schroeder BC, Cheng T, Jan YN, Jan LY. Expression cloning of TMEM16A as a calcium-activated chloride channel subunit. Cell. 2008; 134:1019–1029. [PubMed: 18805094]
43. Schroeder JI, Keller BU. Two types of anion channel currents in guard cells with distinct voltage regulation. Proc. Natl. Acad. Sci. USA. 1992; 89:5025–5029. [PubMed: 1375754]
44. Meyer S, et al. AtALMT12 represents an R-type anion channel required for stomatal movement in Arabidopsis guard cells. Plant J. Jul 12.2010 Epub ahead of print.
45. Sasaki T, et al. Closing plant stomata requires a homolog of an aluminum-activated malate transporter. Plant Cell Physiol. 2010; 51:354–65. [PubMed: 20154005]
46. Punta M, et al. Structural genomics target selection for the New York Consortium on Membrane Protein Structure. J. Struct. Funct. Genomics. 2009; 4:255–268. [PubMed: 19859826]
47. Papadopoulos JS, Agarwala R. COBALT: constraint-based alignment tool for multiple protein sequences. Bioinformatics. 2007; 23:1073–1079. [PubMed: 17332019]
48. Landau M, et al. ConSurf 2005: the projection of evolutionary conservation scores of residues on protein structures. Nucleic Acids Res. 2005; 33:W299–W302. [PubMed: 15980475]
49. Rocchia W, et al. Rapid grid-based construction of the molecular surface for both molecules and geometric objects: applications to the finite difference Poisson-Boltzmann method. J. Comp. Chem. 2002; 23:128–137. [PubMed: 11913378]
50. Altschul SF, et al. Gapped BLAST and PSI-BLAST: a new generation of protein database search programs. Nucleic Acids Res. 1997; 25:3389–3402. [PubMed: 9254694]
51. Kendrick BS, Kerwin BA, Chang BS, Philo JS. Online size-exclusion high-performance liquid chromatography light scattering and differential refractometry methods to determine degree of polymer conjugation to proteins and protein-protein or protein-ligand association states. Anal. Biochem. 2001; 299:136–146. [PubMed: 11730335]
52. Otwinowski Z, Minor W. Processing of X-ray diffraction data collected in oscillation mode. Methods Enzymol. 1997; 276:307–326.
53. Pape P, Schneider TR. HKL2MAP: a graphical user interface for phasing with SHELX programs. J. Appl. Cryst. 2004; 37:843–844.
54. Perrakis A, Morris R, Lamzin VS. Automated protein model building combined with iterative structure refinement. Nat. Struct. Biol. 1999; 6:458–463. [PubMed: 10331874]
55. Emsley P, Cowtan K. COOT: model-building tools for molecular graphics. Acta Crystallogr. D. 2004; 60:2126–2132. [PubMed: 15572765]
56. CCP4. The CCP4 suite: programs for protein crystallography. Acta Crystallogr. D. 1994; 50:760–763. [PubMed: 15299374]
57. Fatt P, Ginsborg BL. The ionic requirements for the production of action potentials in crustacean muscle fibers. J. Physiol. 1958; 142:516–543. [PubMed: 13576452]

58. DeLano, WL. The PyMOL molecular graphics system. DeLano Scientific; San Carlos, CA, USA: 2002. http://www.pymol.org

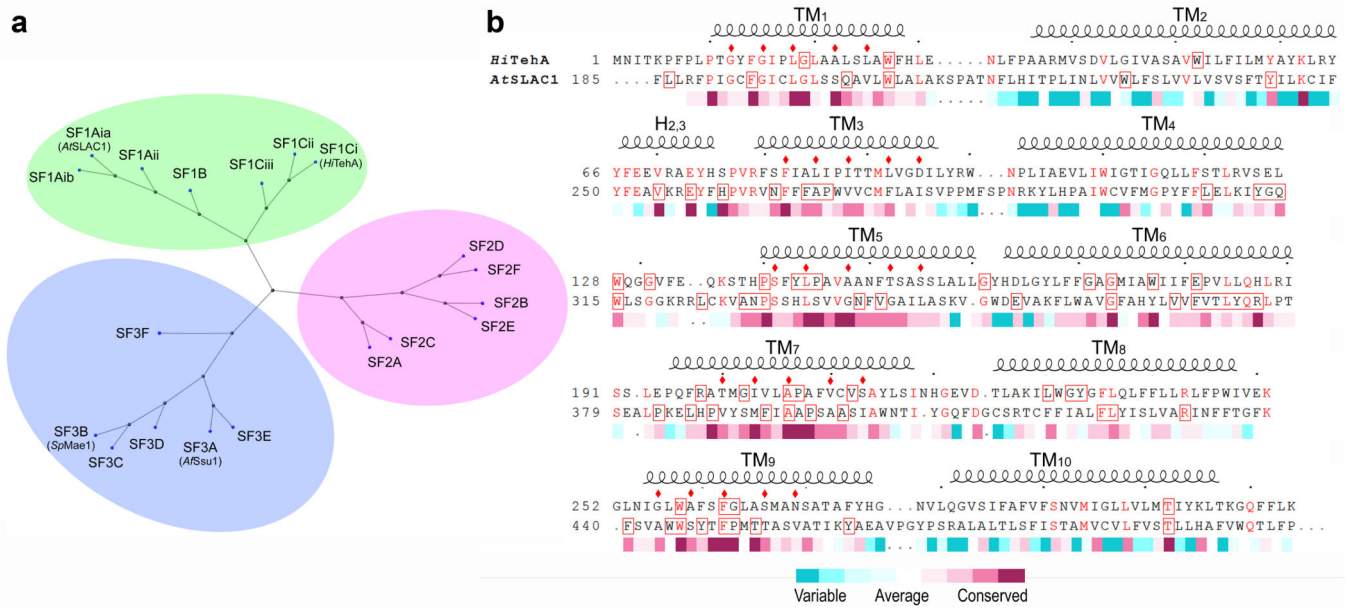

Figure 1. Sequence analysis for the SLAC1 superfamily

a, Family tree. The presentation was computed by the program COBALT[47] from representative subfamily sequences (Table S1), including *Arabidopsis thaliana* SLAC1 for SF1Ai, *Haemophilus influenzae* TehA for SF1Ci, *Escherichia coli* TehA for SF1Cii, *Vibrio parahaemolyticus* for SF2A, *Staphylococcus aureus* for SF2B, *Aspergillus fumigatus* Ssu1 for SF3A, and *Schizosaccharomyces pombe* Mae1 for SF3B. **b,** Structure-based sequence alignment of TehA from *Haemophilus influenzae* (*Hi*TehA) and SLAC1 from *Arabidopsis thaliana* (*At*SLAC1). The TehA structure has been used to restrict sequence gaps to inter-helical segments. Superior coils define extents of the *Hi*TehA helical segments; red letters mark residue identities; red boxes are drawn for residues that are >95% identical within the plant subfamily SF1A for *At*SLAC1 or within the TehA subfamily for *Hi*TehA; red diamonds mark *Hi*TehA residues that line the central pore; and the colored inferior bar encodes ConSurf sequence variability[48] for the SF1 family of 204 non-redundant proteins.

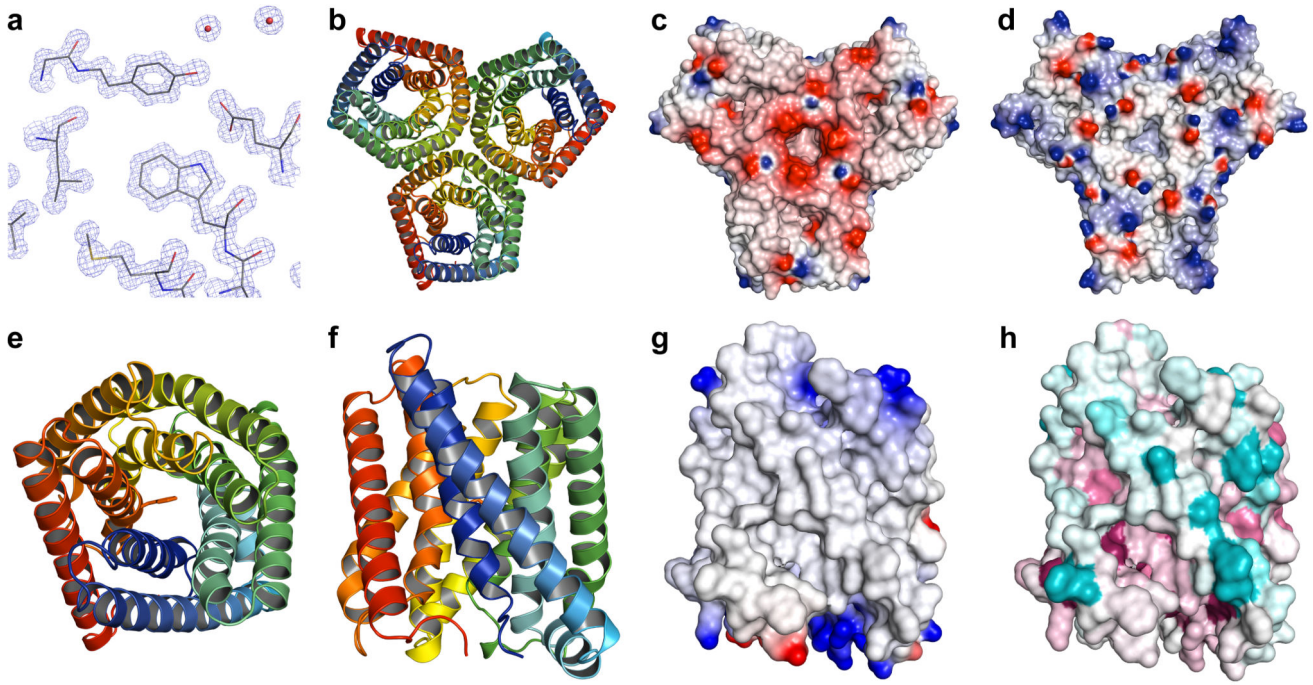

Figure 2. Crystal structure of *Hi*TehA and homology model of *At*SLAC1

a, Electron density distribution from the *Hi*TehA crystal structure at 1.2Å resolution. The map has (2Fo-Fc) coefficients based on the superimposed model. Contours are at 2.5σ. **b,** Ribbon diagram of the *Hi*TehA trimer. Each protomer is colored spectrally from blue at its N-terminus to red at its C-terminus. **c,** DelPhi[49] electrostatic potential at the extracellular surface. Electronegative and electropositive potential are colored in degrees of red and blue saturation, respectively. **d,** Electrostatic potential[49] at the intracellular surface. **e,** Ribbon diagram of an *Hi*TehA protomer viewed from outside the membrane. The ribbon is colored spectrally as in **2b**. **f,** Ribbon diagram of an *Hi*TehA protomer viewed from within the membrane from below the view of **e**. **g,** Surface of a homology model of *At*SLAC1, viewed as in **f**, and colored by sequence variability[48]. **h,** Surface of *At*SLAC1 as in **g**, but colored by electrostatic potential[49].

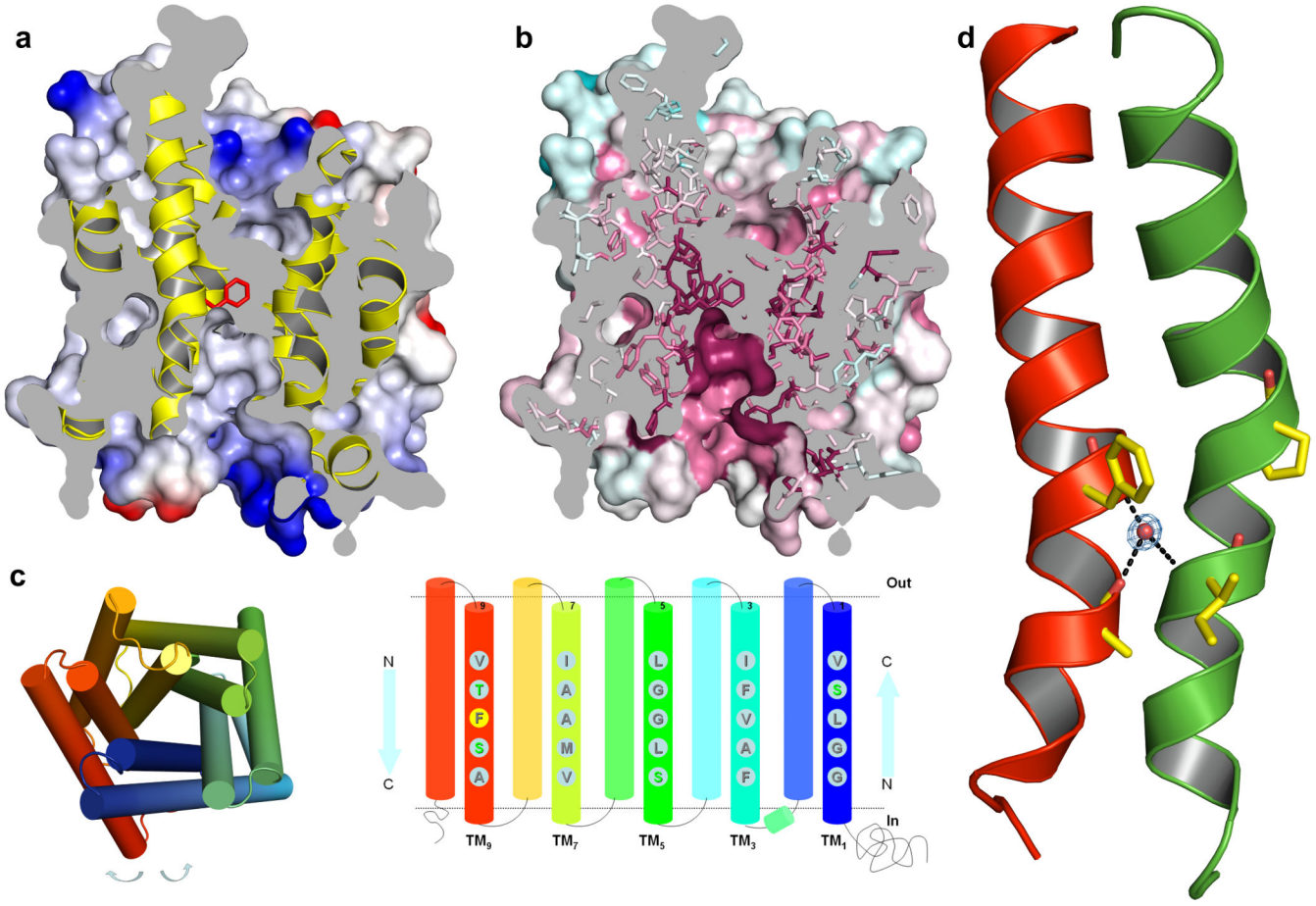

Figure 3. Putative structure of the SLAC1 conductance pore

a, Cross-section through the homology model of *At*SLAC1. The model is viewed as in **2i,** with the electrostatic potential[49] shown on the external surface of the molecular envelope. The side chain of Phe450 is shown as a stick model (red) on the backbone ribbon colored yellow. **b,** Cross-section as in **a,** but colored by surface conservation[48] as in **2h**. **c,** Pore-lining residues in the SLAC1 homology model. A cylinder model (left), spectrally colored as in **2b**, provides a key for viewing the rolled-open structure (left) with pore-lining residues of *At*SLAC1 shown on the TM_{odd} helices. **d,** Ribbon diagrams of *Hi*TehA TM_9 (left) and TM_7 (right) viewed from within the conductance pore. The side chains of Pro207 and Phe262 are shown as well as a kink-stabilizing water HOH25 that is coordinated by the NH of Gly263 and by C=O groups of Gly202 and Ala259. Density contours are shown for the water molecule.

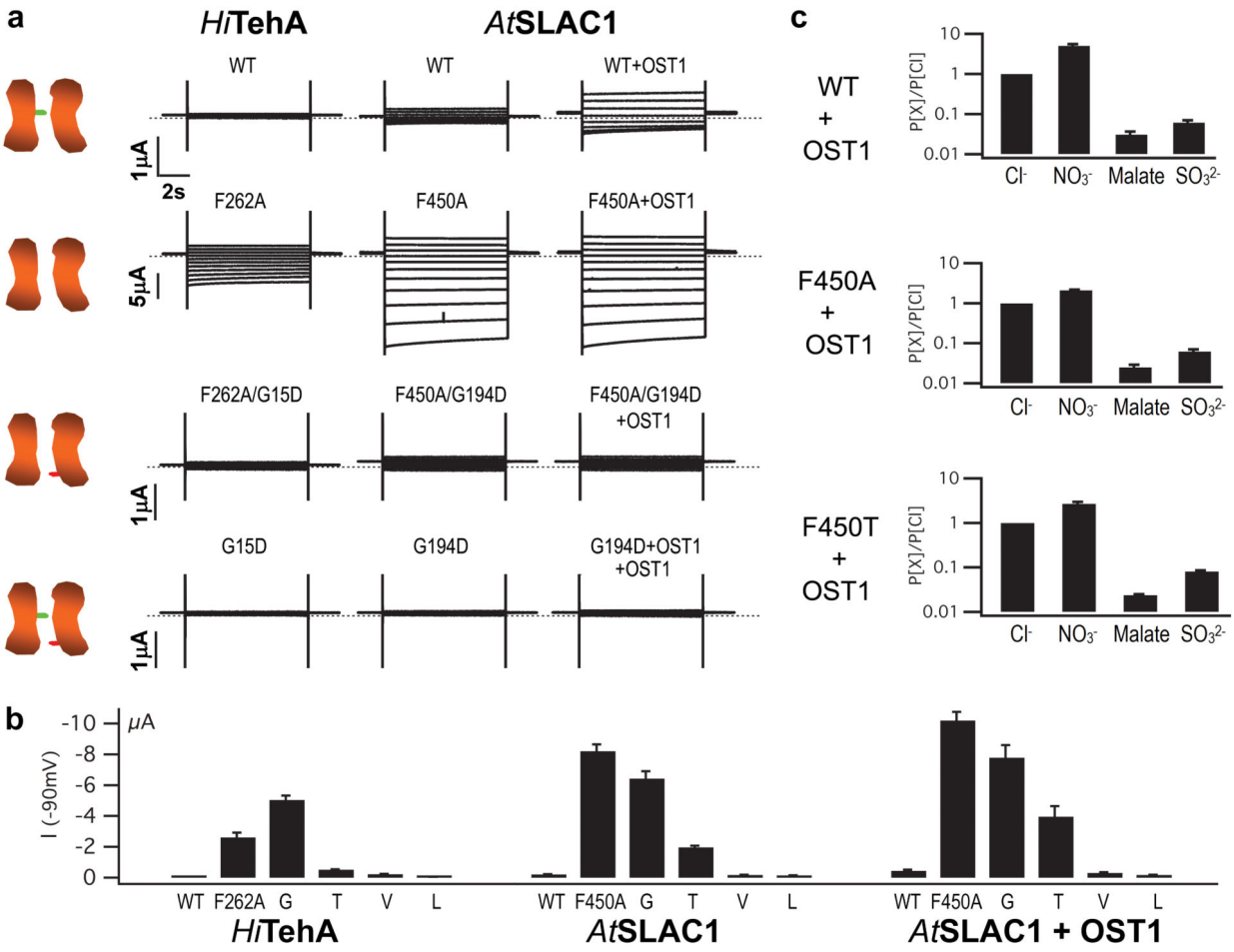

Figure 4. Ionic conductance measurements

a, Typical microelectrode voltage-clamp current traces from oocytes injected with various channel cRNAs. Left column, oocytes injected with cRNAs encoding wild-type *Hi*TehA channels (WT), or F262A, G15D/F262A or G15D mutants. Right two columns, oocytes injected with cRNAs for WT *At*SLAC1, or F450A, G194D/F450A or G194D mutants, with or without co-injection of *At*OST1. Dotted lines represent zero current levels. Extracellular solution contained 30mM CsCl. Schematic keys at the left place phenyl and/or aspartyl gates. **b,** Effects of gating residue mutations. Mean chloride currents, measured at −90 mV, are shown comparing WT *Hi*TehA and its mutant series F262A,G,T,V,L with WT *At*SLAC1 and its corresponding series F450A,G,T,V,L, both alone and co-expressed with *At*OST1. Full I-V relations are shown in Fig. S5. **c,** Effect of gating residues on relative *At*SLAC1 anion permeabilities. Relative permeabilities (P[X]/P[Cl]) for chloride, nitrate, sulfite and malate of WT, F450A and F450T SLAC1 channels were measured from the change in current reversal potential with Cl^- or anion X^- as the sole permeant anion in the bath solution (Methods, Table S6).

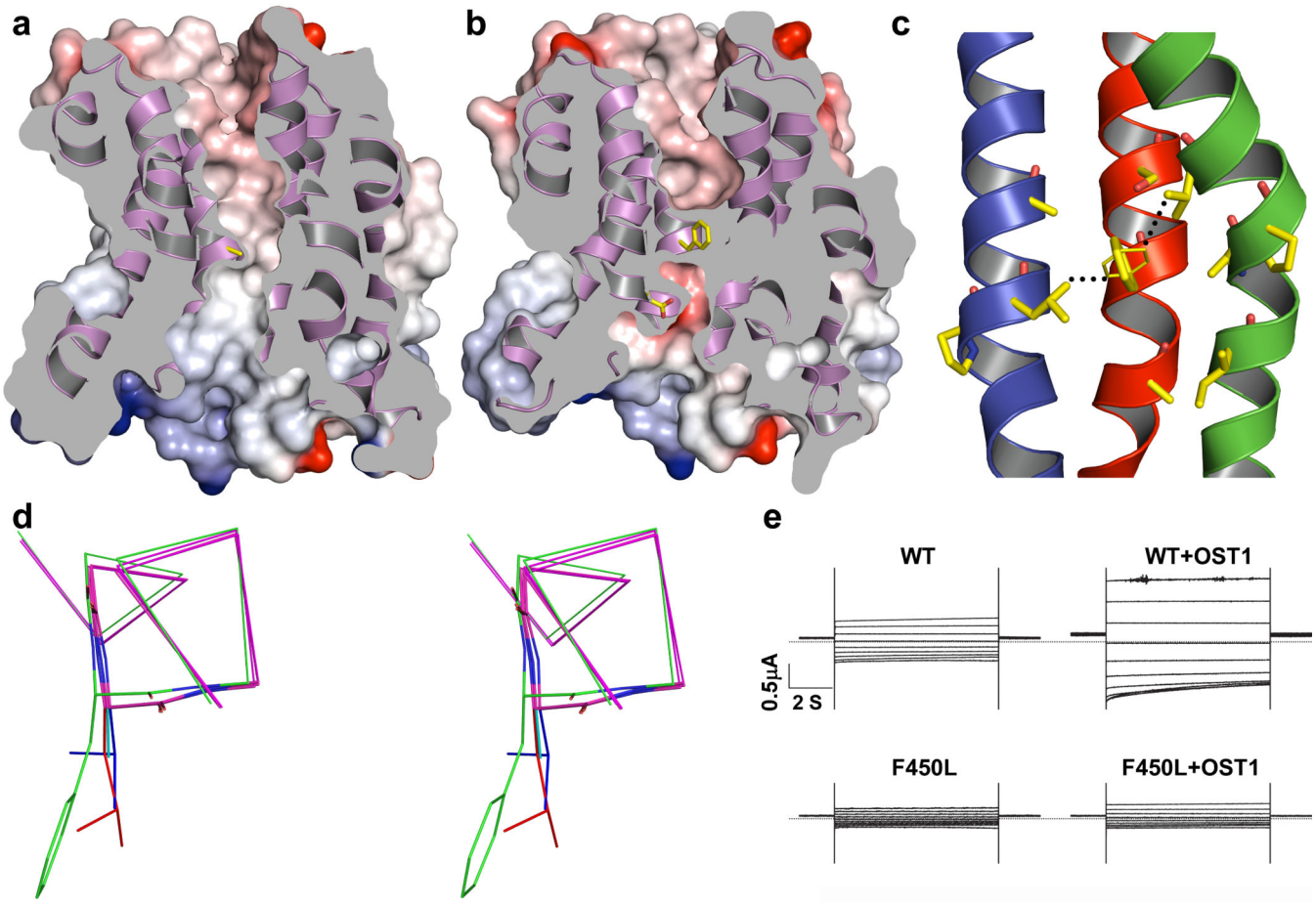

Figure 5. Structural features at the SLAC1 homolog gate

a,b, Cross-sections through the conductance pores of *Hi*TehA F262A and *Hi*TehA G15D. The view and presentations are as in **3a,** except that helices are colored purple. **c,** Molecular basis for conformational strain in gating residue Phe262 of *Hi*TehA. Helices TM_1 (left), TM_9 (center) and TM_7 (right) are viewed from within the pore and presented as ribbon diagrams with selected side chains drawn in stick representation. The local low-energy conformation for the phenyl ring ($\chi_2 = 90°$) is shown in thin lines with short contacts indicated in dashed lines: Leu18 $C_{\delta 2}$ – Phe262 $C_{\delta 1}$, d = 2.4 Å; Val210 $C_{\gamma 2}$ – Phe262 $C_{\varepsilon 2}$, d = 2.8 Å. **d,** Conformational shifts consequent to release of strain in gating residue Phe262. Cα backbone structures of F262A, F262V and F262L *Hi*TehA were first superimposed onto WT *Hi*TehA, and residues 258-266 were drawn in stereo as superimposed. All backbone atoms are shown for peptides 262±1, but only Cα atoms are shown otherwise. The WT backbone and phenyl group are green; other backbone are all magenta; side chains of Ala262, Val262 and Leu262 are cyan, blue and red, respectively; oxygen-directed bonds are red and nitrogen-directed bonds are blue. **e,** Typical microelectrode voltage-clamp current traces from oocytes injected with wild-type (WT) or F450L *At*SLAC1 cRNA. Experimental conditions and displays are as in **4a**.